

Air quality over the Canadian oil sands: A first assessment using satellite observations

C. A. McLinden,¹ V. Fioletov,¹ K. F. Boersma,^{2,3} N. Krotkov,⁴ C. E. Sioris,¹ J. P. Veefkind,^{2,5} and K. Yang^{4,6}

Received 14 November 2011; revised 17 January 2012; accepted 22 January 2012; published 22 February 2012.

[1] Results from the first assessment of air quality over the Canadian oil sands—one of the largest industrial undertakings in human history—using satellite remote sensing observations of two pollutants, nitrogen dioxide (NO₂) and sulfur dioxide (SO₂), are presented. High-resolution maps were created that revealed distinct enhancements in both species over an area (roughly 30 km × 50 km) of intensive surface mining at scales of a few kilometers. The magnitude of these enhancements, quantified in terms of total mass, are comparable to the largest seen in Canada from individual sources. The rate of increase in NO₂ between 2005 and 2010 was assessed at 10.4 ± 3.5%/year and resulted from increases both in local values as well as the spatial extent of the enhancement. This is broadly consistent with both surface-measurement trends and increases in annual bitumen production. An increase in SO₂ was also found, but given larger uncertainties, it is not statistically significant. **Citation:** McLinden, C. A., V. Fioletov, K. F. Boersma, N. Krotkov, C. E. Sioris, J. P. Veefkind, and K. Yang (2012), Air quality over the Canadian oil sands: A first assessment using satellite observations, *Geophys. Res. Lett.*, 39, L04804, doi:10.1029/2011GL050273.

1. Introduction

[2] Vast deposits of bitumen—oil mixed with sand, clay, and water generally referred to as “oil sands” (or “tar sands”)—are located in the Canadian province of Alberta (see Figure 1a). The oil sands are estimated to contain the equivalent of 170 billion barrels (roughly 2.7 × 10⁷ m³) of oil, making it the second-largest reserve globally. About 20% resides in near-surface deposits that may be recovered through surface, or open-pit, mining. Deeper deposits (>100 m) require in-situ extraction techniques. It is only within the past decade or so, however, that increases in the price of oil combined with advances in technology have made extraction of bitumen, and its upgrade into synthetic crude oil, financially viable. In 2010, the oil sands produced the equivalent of 1.8 million barrels of oil per day (mBPD) from bitumen, a number expected to rise to 3.9 mBPD by 2020 with annual

capital expenditure increasing from Cdn\$13 billion to nearly \$20 billion over this period [*Energy Resources Conservation Board (ERCB)*, 2011].

[3] There are a variety of environmental and health concerns associated with oil sands development and operations [e.g., *Kelly et al.*, 2010], including air quality and acid deposition. Combustion of fossil fuel releases nitrogen oxides while sulfur is released from the mine face, tailings ponds, and the bitumen during upgrading. The sheer scale of operations, its rapid expansion, and massive energy requirements to extract and upgrade the bitumen, has led to concerns over air pollution at and downwind of site locations. A recent flight of the NASA DC-8 research aircraft sampled air over the oil sands that was significantly enhanced in nitrogen dioxide (NO₂), sulfur dioxide (SO₂), and many other species [*Simpson et al.*, 2010]. These data represent the exception as there are few published studies examining the air quality in this region. The Wood Buffalo Environmental Association (WBEA, www.wbea.org) performs monitoring at several surface stations throughout the oil sands. While these data are publicly available, their compliance-monitoring mandate has meant they have not been vetted in peer-reviewed publications.

[4] An alternative and complementary approach to surface and aircraft measurements is monitoring from satellites. This has proven to be of enormous benefit to our understanding of the global distribution, sources, and trends of pollutants such as NO₂ and SO₂ [e.g., *Martin et al.*, 2003; *Richter et al.*, 2005]. The majority of this work, however, has been on regional or continental scales. Investigation of sources with spatial scales comparable to or smaller than the spatial resolution of the sensor represents an additional challenge that has only recently been addressed [*Kim et al.*, 2009; *Fioletov et al.*, 2011; *Beirle et al.*, 2011]. Furthering these studies, this work is the first to assess air quality over the oil sands using satellite remote sensing observations of NO₂ and SO₂.

2. Satellite Observations of Air Quality

[5] Global monitoring by satellite of tropospheric pollutants began with the GOME (Global Ozone Monitoring Experiment, 1996–2003) instrument, a UV-visible nadir spectrometer [*Burrows et al.*, 1999]. Successors to GOME include SCIAMACHY (SCanning Imaging Absorption spectroMeter for Atmospheric Cartography, 2002-present) [*Bovensmann et al.*, 1999], OMI (Ozone Monitoring Instrument, 2004-present) [*Levelt et al.*, 2006], and the operational GOME-2 (2007-present) instrument. These instruments derive the vertical column density (VCD) of gases such as NO₂ and SO₂ by measuring UV-visible solar radiation in nadir (down-looking) geometry. Processing of the data from calibrated

¹Environment Canada, Toronto, Ontario, Canada.

²Royal Netherlands Meteorological Institute, De Bilt, Netherlands.

³Fluid Dynamics Laboratory, Eindhoven University of Technology, Eindhoven, Netherlands.

⁴Laboratory for Atmospheric Chemistry and Dynamics, NASA Goddard Space Flight Center, Greenbelt, Maryland, USA.

⁵Civil Engineering and Geosciences, Delft University of Technology, Delft, Netherlands.

⁶Department of Atmospheric and Oceanic Sciences, University of Maryland, College Park, Maryland, USA.

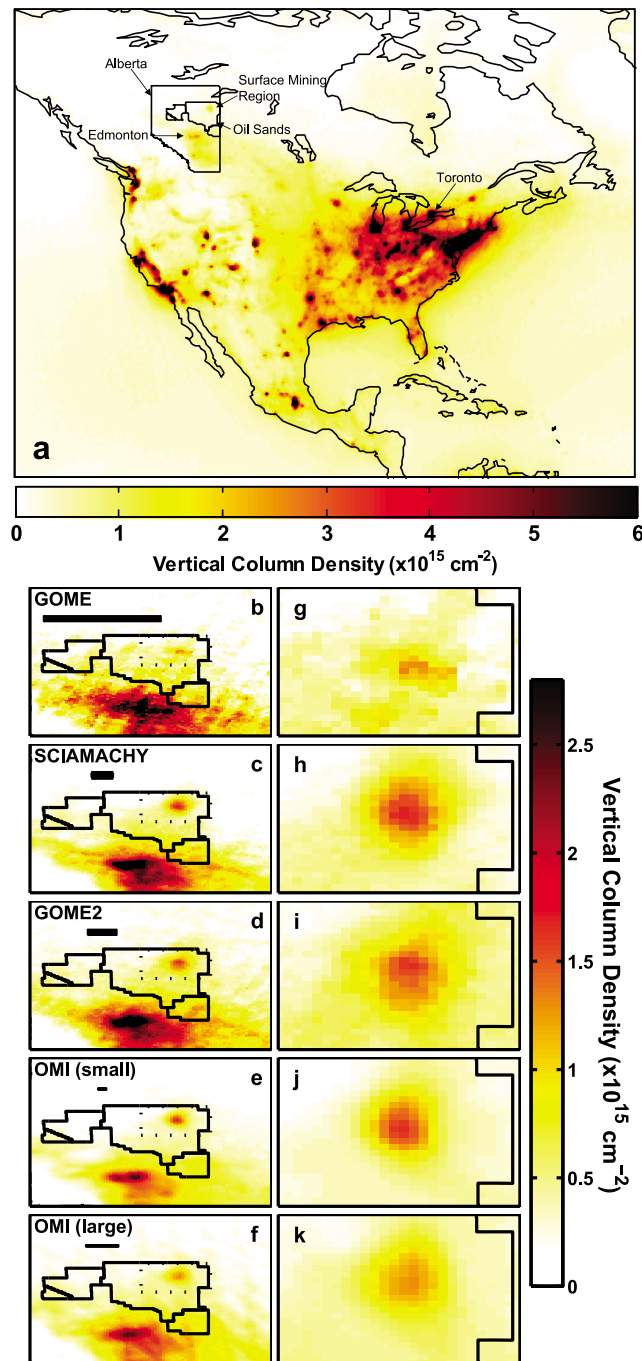


Figure 1. Tropospheric vertical column densities (VCDs) of NO_2 : (a) OMI annual mean VCD (2004–2010) over North America averaged onto a $0.25^\circ \times 0.25^\circ$ grid; (b–f) mission average annual VCDs for GOME, SCIAMACHY, GOME-2, and OMI using $8 \text{ km} \times 8 \text{ km}$ grid with a 20 km averaging radius (see text) over the oil sands (see box in Figure 1a); Below each sensor name is a solid rectangle representing the approximate size of a resolution element, or pixel, for that instrument. (g–k) The outline in each panel represents the borders of the oil sands regions and the dotted box shows the areas that are further enlarged; Figures 1g–1k are an enlargement of Figures 1a–1f over the area of extensive surface mining.

spectra to tropospheric VCDs involves three main steps [e.g., *Boersma et al.*, 2007]: (i) a spectral fit to obtain the total, slant-path-integrated column density (SCD), (ii) removal of the stratospheric contribution to the SCD, and (iii) a conversion to tropospheric VCD using a radiative transfer model that accounts for the complex path of scattered and reflected sunlight.

[6] A key difference among these four sensors is their horizontal resolution, given in Table 1. For example, there is a factor of 40 difference between the surface area sampled in a single observation, or ‘pixel’, between GOME ($40 \times 320 \text{ km}^2$) and OMI ($13 \times 24 \text{ km}^2$). Unlike the others, OMI does not need to scan across track but rather it uses a two-dimensional detector that measures simultaneously at 60 across-track positions. Its across-track resolution varies significantly with track position: those pixels near the track centre (corresponding to nadir) are roughly 30 km wide while those near the edge are $>100 \text{ km}$ wide. A so-called ‘row anomaly’ beginning in 2007 has meant some track positions are no longer reliable (see <http://www.knmi.nl/omi/research/product/rowanomaly-background.php>).

[7] In this analysis, NO_2 data from all four instruments were examined. While different NO_2 data products are available, the only one consistent across all four sensors is the Dutch KNMI algorithm (TM4NO2A, version 2, <http://www.temis.nl/airpollution/no2.html>) [*Boersma et al.*, 2011], and so was chosen for this application. Analysis of SO_2 data were limited to the OMI instrument (OMSO2, version 3, http://disc.sci.gsfc.nasa.gov/Aura/data-holdings/OMI/omso2_v003.shtml) [*Krotkov et al.*, 2006]. In all cases level 2 (orbit-based) data were used in which the location of an observation was assigned to the co-ordinates of the pixel center. Only data with a cloud fraction of 0.2 or less were retained and a solar zenith angle limit of $75^\circ/60^\circ$ was placed on NO_2/SO_2 . Data from OMI track positions affected by the row anomaly were also excluded for both species. Year-round NO_2 data were used but, following *Fioletov et al.* [2011], only summertime (May–August) SO_2 data were used as they possess the best signal-to-noise and also were limited to $\leq 5 \text{ DU}$ ($1 \text{ DU} = 2.69 \times 10^{16} \text{ molecules/cm}^2$) to exclude volcanic plumes. It is noted here that the number of (cloud-filtered) NO_2 observations over the oil sands is roughly constant throughout the year.

3. Observations of NO_2 and SO_2 Over the Oil Sands

[8] Figure 1a shows North American, annual-mean OMI tropospheric NO_2 VCDs (2005–2010) averaged onto a $0.25^\circ \times 0.25^\circ$ grid. The oil sands region within Alberta is indicated and on this continental scale only a relatively small enhancement can be seen here. This region is examined in greater detail using the pixel averaging technique described by *Fioletov et al.* [2011]. A fine spatial grid was defined, initially $8 \times 8 \text{ km}^2$. All screened observations from a sensor, within a given time window and falling within a radius of 20 km from the grid-cell center, were averaged. Averaging observations from a large number of satellite overpasses, each at a slightly different location, allows greater detail such as the center and shape of the enhancement to be resolved. This assumes that the source is relatively constant over the averaging period.

Table 1. Summary of Datasets and Analysis Over Oil Sands Region^a

Species	Instrument	Data Product	Period Used	Horizontal Resolution	Enhancement		Data Points Within 15 km ^b (/yr)
					Mass (tonnes)	Radius (km)	
NO ₂	GOME	TM4NO2A V2.0	1996–2003	40 × 320	6.6 ± 5.1	33.5 ± 20.4	2.5
NO ₂	SCIAMACHY	TM4NO2A V2.0	2002–2010	30 × 60	6.2 ± 0.9	28.4 ± 3.2	11
NO ₂	GOME-2	TM4NO2A V2.1	2007–2010	40 × 80	7.1 ± 1.3	33.4 ± 5.1	29
NO ₂	OMI	DOMINO V2.0	2004–2010	13 × 33 ^c	4.5 ± 0.2	25.4 ± 0.8	190 (91) ^d
SO ₂	OMI	NASA OMSO2 V003	2004–2010	13 × 33 ^c	28.8 ± 12.5	22.3 ± 7.1	196 (98) ^d

^aRadius is the geometric mean of the two fitted width parameters.

^bRelative to Mildred Lake (57.0°N, 111.6°W).

^cApproximate median across-track resolution.

^dConsidering small (large) OMI pixels.

[9] Figures 1b–1f show the area near the oil sands as viewed by the GOME, SCIAMACHY, GOME-2, and OMI instruments. (Each ‘square’ in these plots is 8 × 8 km².) The large NO₂ enhancement near the bottom of these panels is from the city of Edmonton (400 km from the oil sands) and nearby industry. Also shown in each panel is a solid rectangle that represents the approximate pixel size of that sensor. Two OMI maps are shown—one considering only ‘small’ OMI pixels (track positions 11–50) and one considering only ‘large’ (1–10, 51–60) [Levelt *et al.*, 2006]. The spatial scale of these panels is further reduced in Figures 1g–1k and centered on the surface mining region. Despite a large difference in pixel size, SCIAMACHY, GOME-2, and OMI present a consistent picture of the oil sands: an elliptical-shaped enhancement region, roughly 30 × 50 km², with a maximum of roughly 2 × 10¹⁵ molecules/cm². The greater detail observed in the OMI panels is consistent with its finer resolution and larger number of observations. Note that some differences are expected owing to (i) overpass times—OMI observes early afternoon while the others observe mid-morning, and (ii) the different periods over which each sensor has data (see Table 1). As a result of its large pixel size and dearth of data points in the immediate vicinity of the enhancement (see Table 1), GOME is able to only partially resolve the NO₂ enhancement, although since it spans the earlier period 1996–2003, there may in fact be less to resolve. This requires further investigation. The overall consistency between the other instruments, however, suggests that lower-resolution instruments such as GOME-2 can still be used to monitor local sources (at coarser resolution) provided there are sufficient observations.

[10] With its superior resolution and high volume of observations, OMI allows this methodology to be pushed further: the OMI data were reanalyzed using a 1 × 1 km² grid, averaging over an 8 km radius. This map is shown in Figure 2a. The ellipse in Figure 1 gives way to two regions of enhancement: a larger maximum in the south located over the Syncrude Canada Mildred Lake and Suncor Energy Millennium surface mining operations (indicated in Figure 2a), two significant sources of NO₂ according to the National Pollution Release Inventory (NPRI) database (NPRI, Nitrogen oxide and sulfur oxide emissions for Canada, 2011, accessed 8 August 2011, available at http://www.ec.gc.ca/pdb/websol/querysite/query_e.cfm), and a smaller maximum in the north. The same procedure was applied to OMI SO₂ data, but using a 2 × 2 km² grid and a 24 km averaging radius, with the larger radius being necessary due to the higher noise levels in the SO₂ product. From Figure 3a, an SO₂ enhancement over the Syncrude Mildred Lake and Suncor operations is also

evident, with a peak of 0.45 DU. Relative to NO₂, it appears somewhat elongated in the E–W direction and without a secondary maximum in the north. This is consistent with the various operations in the oil sands region: Syncrude-Mildred Lake and Suncor have on-site upgrade facilities that are responsible for the bulk of the SO₂ emissions and some of the NO₂ emissions. While surface mining is also carried out in the northerly area, the bitumen from this area is piped elsewhere for upgrading. Hence much smaller SO₂ emissions would be expected here whereas the secondary NO₂ maximum is likely the result of emissions from the extraction and transport (including the “heavy hauler” trucks) sources that do not report to NPRI.

4. Evolution and Trends

[11] The evolution of the NO₂ distribution can be studied by averaging separately over two time periods: 2005–2007 and 2008–2010. However, two small but systematic effects were identified that, if unaccounted for, would bias comparisons between these two periods (see the auxiliary material for details).¹ According to data from the Moderate Resolution Imaging Spectrometer (MODIS), surface reflectivity was seen to increase by about 0.006 between 2005 and 2010 as a result of changing land cover. Likewise, aerosol optical depth also increased from 0.14 to 0.21 over this same period. As discussed in the auxiliary material, both these parameters impact the air mass factors but have not been accounted for in the OMI retrieval algorithm. Correction factors appropriate for each month from 2005–2010 were derived and applied to each OMI NO₂ VCD. The magnitude of the correction was always less 20% and they were normalized so they did not impact the 2005–2010 mean VCD. Only corrected NO₂ VCDs were considered throughout the remainder of this study.

[12] Comparing the 2005–2007 (Figure 2b) with the 2008–2010 (Figure 2c) mean NO₂ VCD, an increase in NO₂ with time is evident. Two approaches were used in an attempt to verify this increase. The first involves SCIAMACHY data. Analogous maps for the periods 2003–2006 and 2007–2010 were generated using an averaging radius of 15 km and they show a similar increase with time (see insets in Figures 2b and 2c). The second makes use of in-situ measurements of NO₂ recorded at five WBEA monitoring stations (locations indicated in Figures 2a–2c; see the auxiliary material for further details). Seasonally-averaged time series

¹Auxiliary materials are available in the HTML. doi:10.1029/2011GL050273.

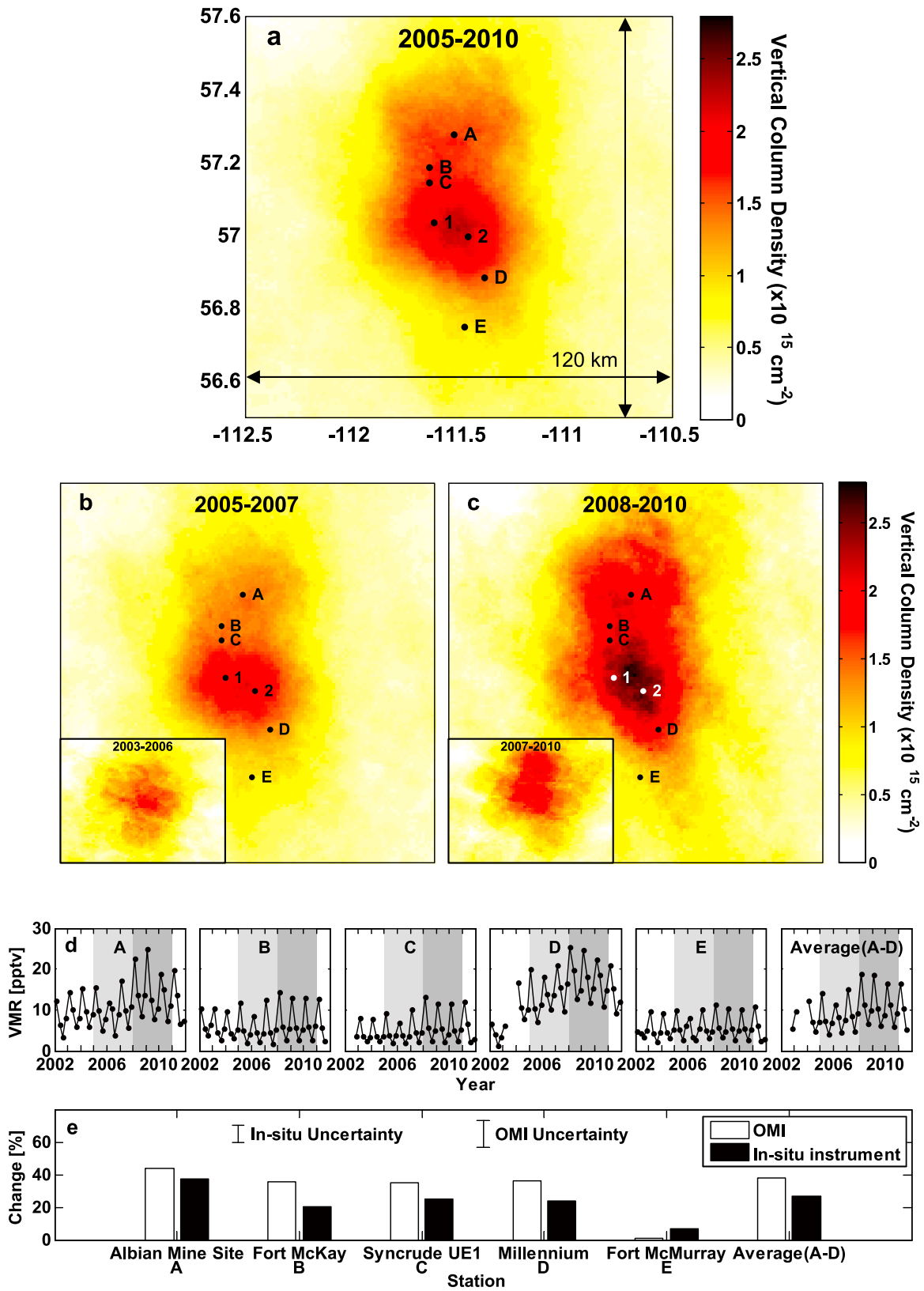


Figure 2

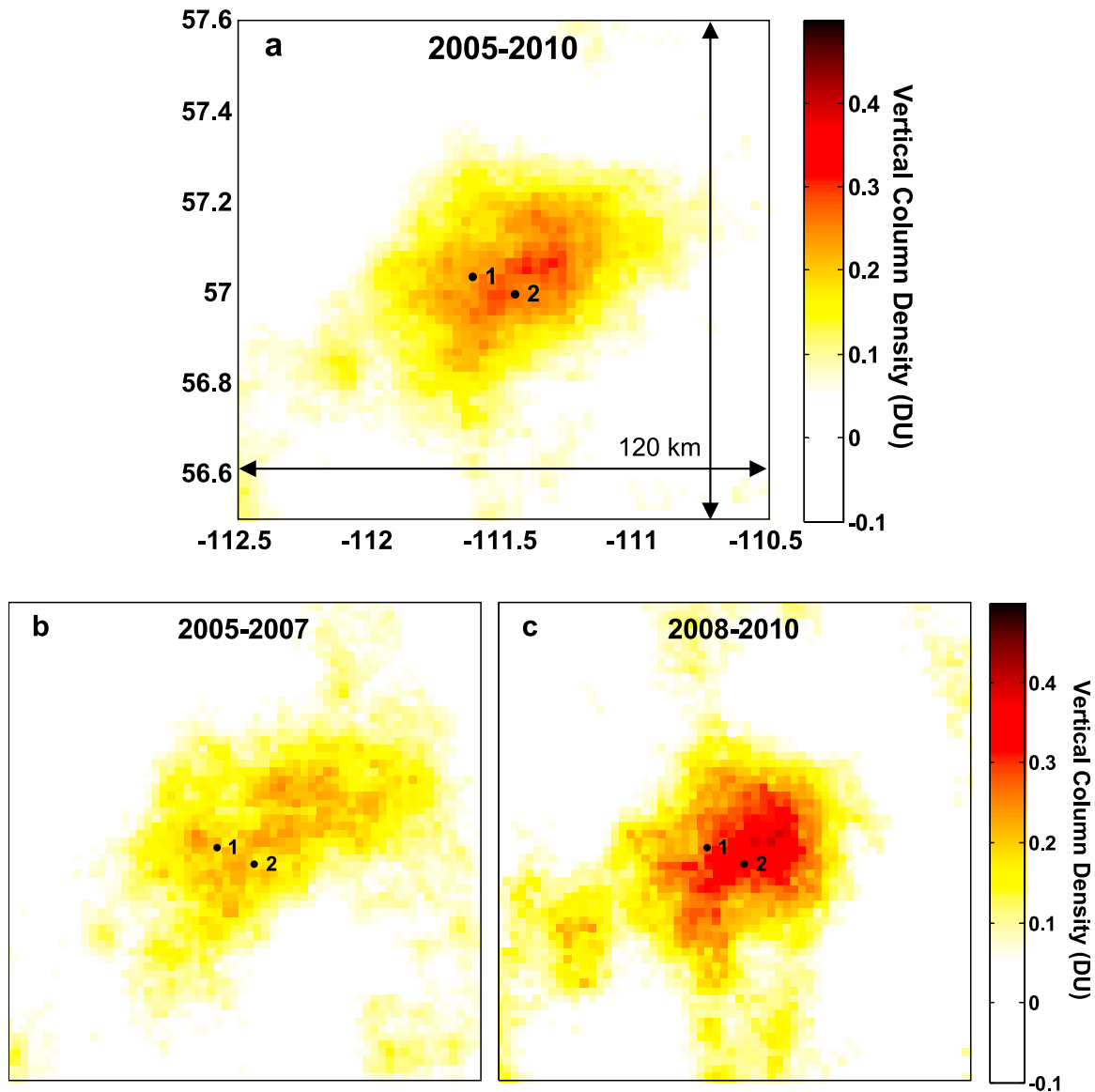


Figure 3. (a) OMI annual mean tropospheric SO₂ VCD, averaged over 2005–2010 shown on a 2×2 km² grid and calculated using an averaging radius of 24 km. Large SO₂ emission sources reporting to NPRI (http://www.ec.gc.ca/pdb/websol/querysite/query_e.cfm) are Syncrude (denoted with ‘1’) and Suncor (‘2’). (b and c) As Figure 3a but separated into 2005–2007 and 2008–2010 averaging periods.

of NO₂ volume mixing ratio (vmr) at these stations, measured by chemiluminescence detectors (CASA, 2011, <http://www.casadata.org/Reports/SelectCategory.asp>), are shown in Figure 2d. The two periods under consideration are highlighted, and there is a clear increase in the second

period relative to the first at the four stations located near surface mines. Direct comparisons between OMI and in-situ measurements are difficult, but the consistency in their relative changes between these two periods can be assessed. In the case of OMI, the relative difference between the two

Figure 2. (a) OMI annual mean tropospheric NO₂ VCD, averaged over 2005–2010, shown on a 1×1 km² grid and calculated using an averaging radius of 8 km. Large NO₂ emission sources reporting to NPRI (http://www.ec.gc.ca/pdb/websol/querysite/query_e.cfm) are Syncrude (denoted with ‘1’) and Suncor (‘2’). Monitoring stations equipped with in-situ NO₂ instruments are located at locations A–D. (b and c) As Figure 2a but separated into 2005–2007 and 2008–2010 averaging periods, respectively. Inset: SCIAMACHY averaged over 2003–2006 and 2007–2010 using a 15 km averaging radius. (d) Seasonally-averaged NO₂ volume mixing ratio (vmr) time series as measured at the four monitoring stations, and the mean over all four stations. The gray backgrounds identifies the two averaging periods: 2005–2007 and 2008–2010. The standard error of the mean is 12–18%. (e) The relative change in mean NO₂ between 2008–2010 and 2005–2007 at each station. The OMI change is simply the difference at locations A–D (see Figure 2b) between the two time periods and the in-situ change is the relative difference in vmr averaged over each period. The in-situ and OMI uncertainties are their standard errors, corrected for auto-correlation.

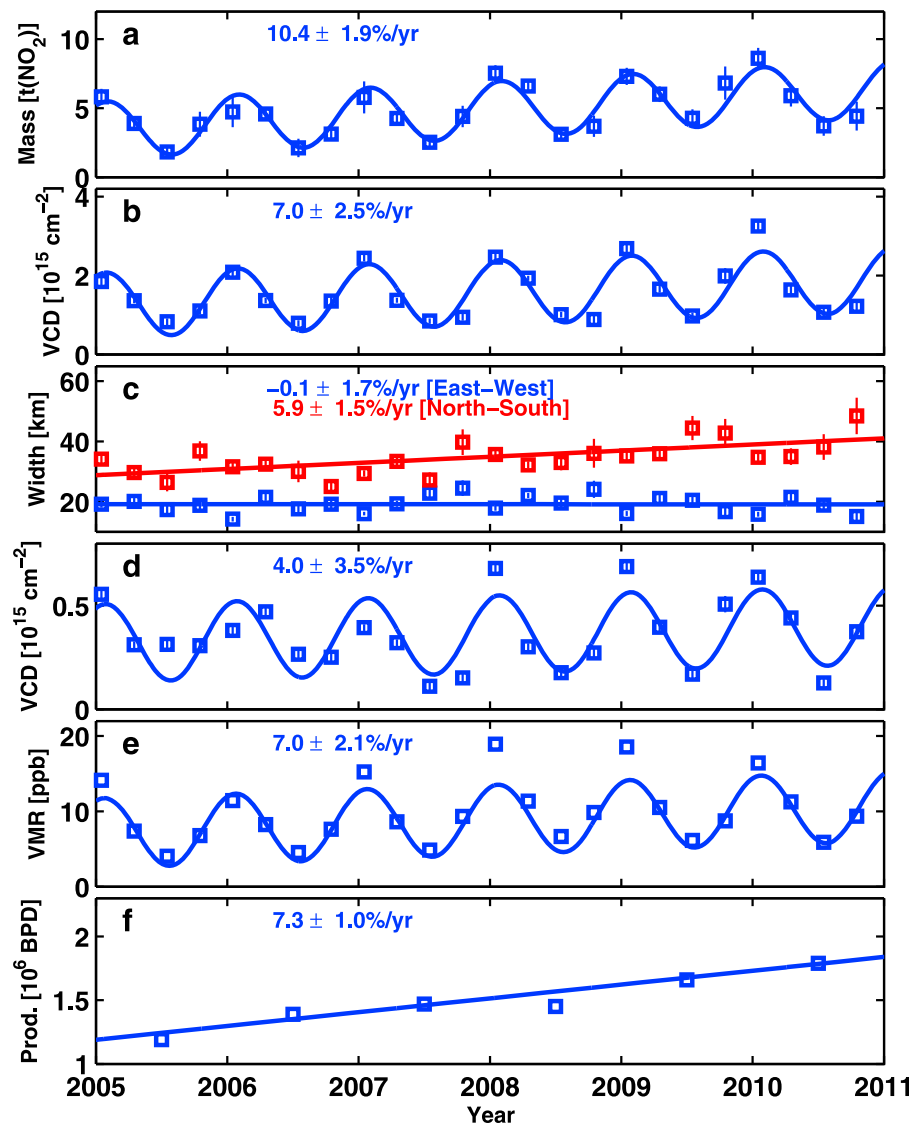


Figure 4. Time series of seasonal OMI NO₂ 2D Gaussian fit parameters: (a) total mass of the NO₂ enhancement in tonnes of NO₂, (b) maximum VCD of the enhancement (c) North–south and East–west width parameters (half-width half-maximum), and (d) background VCD. Also shown are (e) the average seasonal volume mixing ratio time series (from Figure 3d) with a background NO₂ removed (see text) and (f) annual oil sands bitumen production (barrels per day, BPD, of oil equivalent) [ERCB, 2011]. Also shown for each time series are the fits to the time series using a trend model with constant, linear, and annual harmonic terms (except the width and production time series in which only constant and linear terms were used) and the calculated linear trend and trend uncertainties.

maps at the four grid-cells containing the stations in Figures 2b and 2c was calculated. For the in-situ detectors, seasonal values were further averaged over the three-year time intervals and their difference was computed. The results are shown in Figure 2e: the two agree to within measurement uncertainties, with OMI suggesting an average increase of $38 \pm 17\%$ and the in-situ instruments seeing a $27 \pm 11\%$ increase.

[13] OMI SO₂ data also suggests an apparent increase between these two time periods as is evident upon comparing Figures 3b and 3c. However, the higher noise levels in these measurements mean that the difference between these maps is not statistically significant. Surface monitoring of SO₂ is performed by WBEA but these data display high variability (resulting from factors such as local topography and wind

direction) and so a proper analysis is beyond the scope of this paper.

[14] OMI NO₂ data are abundant enough to examine its evolution from a seasonal perspective. This was accomplished using the approach of *Fioletov et al.* [2011] in which VCDs within a 100 km radius of the Syncrude Mildred Lake facility (center: 57.0°N, 111.6°W) were fit to a two-dimensional Gaussian function with a modification made to include a constant offset. The non-linear, least squares fit resulted in seven parameters, including the VCD and location of the maximum, two width parameters, and the background VCD. In principle, the background represents the VCD that would be observed in the absence of emissions from oil sands operations, but it may also contain artefacts from the removal of the stratospheric column. The total mass

of the enhancement (above the background) was calculated by integrating over the Gaussian term. A simple trend model with a constant, linear, and annual harmonic terms was then fit to the resultant time series. Trends were taken as the linear change, relative to the mean, over the time series. Time series and fits from the trend model are shown in Figure 4.

[15] From Figures 4a and 4b, the mass and maximum VCD of the NO₂ enhancement are seen to be increasing at rates of 10.4 ± 1.9 and $7.0 \pm 2.5\%$ /year, respectively. The difference between these values is due to the increased spatial extent of the enhancement, as seen in the increase in the latitudinal (North–south) width parameters in Figure 2c, which impacts the integrated amount. It is noted here that the effect of the AMF correction on the trend in the mass of the enhancement (included in the $10.4\%/yr$) was to reduce it by $1.9\%/yr$. Figure 4d shows an increasing trend in the background VCD but factoring in its large uncertainty it can be taken to be approximately constant with time.

[16] The average vmr time series (from Figure 2d) is replotted in Figure 4e but with a seasonal background removed as derived from a WBEA background site located at Fort Chipewyan (200 km north of the OMI NO₂ maximum; see auxiliary material). After removal of the seasonal background, the trend is found to be $7.0 \pm 2.1\%/year$. This is consistent with the $7.0 \pm 2.5\%/year$ trend in the maximum VCD enhancement from Figure 4b.

[17] As stated previously, the trend in the mass of the NO₂ enhancement is $10.4\%/year$ (2005–2010). However, its uncertainty of $1.9\%/year$ from Figure 4a represents only the statistical uncertainty and is thus a lower limit. An error analysis was performed considering additional sources of uncertainty such as cloud fraction threshold, changing the Gaussian fitting radius, and possible remaining errors in the AMF. This is provided in the auxiliary material. The overall uncertainty was assessed at $3.5\%/yr$.

[18] The rate of increase in annual bitumen production [ERCB, 2011], which could be considered a proxy for NO₂ emissions, is $7.3 \pm 1.0\%/year$ from Figure 4f (see auxiliary material for an expanded time series of production). This is generally consistent with the $10.4 \pm 3.5\%/yr$ trend in mass of the enhancement, which would additionally include a signal from sectors such as construction that do not directly contribute to production.

5. Discussion and Conclusions

[19] A first study of the abundance of NO₂ and SO₂ over the Canadian oil sands, based on UV/visible nadir-viewing satellite instruments, was presented. Using observations from the OMI instrument, maps of each species revealed distinct enhancements, covering roughly $30 \text{ km} \times 50 \text{ km}$, centred over a region of surface mining. Maximum VCDs were found to correspond to the locations of significant emissions from large mining operations.

[20] A trend in the mass of the NO₂ enhancement—the quantity most representative of NO₂ emissions—of $10.4 \pm 3.5\%/yr$ (2005–2010) was found to result from increases in both the maximum VCD and the area of the enhancement. This highlights the importance of satellite observations in providing a macroscopic or comprehensive view.

[21] It is important to provide some context for these results. The OMI SO₂ enhancement over the oil sands is as large as that from any other individual emissions source in

Canada, including the large base-metal smelting operations in Manitoba and Ontario. These results may also be compared with OMI SO₂ enhancements seen near US coal-burning power plants. The map from Fioletov *et al.* [2011] is replotted in the auxiliary material using the same color scale as that used in Figure 3. Values over the oil sands are similar as those of moderate to large power plants with annual emission rates of 100 kt[SO₂]. The situation with NO₂ is somewhat different: while the OMI NO₂ signal is significant and comparable to that measured over large, individual sources such as coal-burning power plants, it is smaller than what is observed over large metropolitan areas. This can be seen in Figure 1. The city of Edmonton, with a population of approximately one million and large power plants and oil refineries nearby, has NO₂ VCDs that are a factor of 2–3 larger and cover a much larger area.

[22] While instruments with coarser resolution such as the operational GOME-2 cannot provide the same level of detail as OMI, they are still useful for integrated monitoring of the oil sands provided sufficient observations exist. On the other hand, planned satellite UV-visible spectrometers such as the European Tropospheric-OMI, NASA GEO-CAPE (Geostationary Coastal and Air Pollution Events), and Canadian Space Agency Polar Communication and Weather missions will all have higher spatial resolution (<10 km) that will enable even greater detailed mapping and monitoring of small-scale point pollution sources.

[23] **Acknowledgments.** The authors thank the Wood Buffalo Environmental Association (WBEA) for the provision of their in-situ data. In particular, CM thanks Kevin Percy of WBEA for helpful discussions. We acknowledge the free use of tropospheric NO₂ column data from the GOME, SCIAMACHY, OMI, and GOME-2 sensors from www.temis.nl. We also acknowledge the NASA Earth Science Division for funding of OMI NO₂ and SO₂ products development and analysis.

[24] The Editor thanks two anonymous reviewers for their assistance in evaluating this paper.

References

- Beirle, S., et al. (2011), Megacity emissions and lifetimes of nitrogen oxides probed from space, *Science*, 333, 1737–1739, doi:10.1126/science.1207824.
- Boersma, K. F., et al. (2007), Near-real time retrieval of tropospheric NO₂ from OMI, *Atmos. Chem. Phys.*, 7, 2103–2118, doi:10.5194/acp-7-2103-2007.
- Boersma, K. F., et al. (2011), An improved tropospheric NO₂ column retrieval algorithm for the Ozone Monitoring Instrument, *Atmos. Meas. Tech.*, 4, 1905–1928, doi:10.5194/amt-4-1905-2011.
- Bovensmann, H., et al. (1999), SCIAMACHY: Mission objectives and measurement modes, *J. Atmos. Sci.*, 56(2), 127–150, doi:10.1175/1520-0469(1999)056<0127:SMOAMM>2.0.CO;2.
- Burrows, J. P., et al. (1999), The Global Ozone Monitoring Experiment (GOME): Mission concept and first scientific results, *J. Atmos. Sci.*, 56, 151–175, doi:10.1175/1520-0469(1999)056<0151:TGOMEG>2.0.CO;2.
- Energy Resources Conservation Board (ERCB) (2011), ST98:2011: Alberta's energy resources 2010 and supply/demand outlook 2011:2020, report, Calgary, Alberta, Canada. [Available at <http://www.ercb.ca/>.]
- Fioletov, V. E., C. A. McLinden, N. Krotkov, M. D. Moran, and K. Yang (2011), Estimation of SO₂ emissions using OMI retrievals, *Geophys. Res. Lett.*, 38, L21811, doi:10.1029/2011GL049402.
- Kelly, E. N., et al. (2010), Oil sands development contributes elements toxic at low concentrations to the Athabasca River and its tributaries, *Proc. Natl. Acad. Sci. U. S. A.*, 107, 16, 178–183, doi:10.1073/pnas.1008754107.
- Kim, S.-W., A. Heckel, G. J. Frost, A. Richter, J. Gleason, J. P. Burrows, S. McKeen, E.-Y. Hsie, C. Granier, and M. Trainer (2009), NO₂ columns in the western United States observed from space and simulated by a regional chemistry model and their implications for NO_x emissions, *J. Geophys. Res.*, 114, D11301, doi:10.1029/2008JD011343.
- Krotkov, N. A., S. A. Carn, A. J. Krueger, P. K. Bhartia, and K. Yang (2006), Band residual difference algorithm for retrieval of SO₂ from the Aura Ozone Monitoring Instrument (OMI), *IEEE Trans. Geosci. Remote Sens.*, 44, 1259–1266, doi:10.1109/TGRS.2005.861932.

- Levelt, P. F., et al. (2006), The Ozone Monitoring Instrument, *IEEE Trans. Geosci. Remote Sens.*, *44*, 1093–1101, doi:10.1109/TGRS.2006.872333.
- Martin, R. V., D. J. Jacob, K. Chance, T. P. Kurosu, P. I. Palmer, and M. J. Evans (2003), Global inventory of nitrogen oxide emissions constrained by space-based observations of NO₂ columns, *J. Geophys. Res.*, *108*(D17), 4537, doi:10.1029/2003JD003453.
- Richter, A., et al. (2005), Increase in tropospheric nitrogen dioxide over China observed from space, *Nature*, *437*, 129–132, doi:10.1038/nature04092.
- Simpson, I. J., et al. (2010), Characterization of trace gases measured over Alberta oil sands mining operations: 76 speciated C₂–C₁₀ volatile organic compounds (VOCs), CO₂, CH₄, CO, NO, NO₂, NO_y, O₃ and SO₂, *Atmos. Chem. Phys.*, *10*, 11,931–11,954, doi:10.5194/acp-10-11931-2010.
- K. F. Boersma and J. P. Veefkind, Royal Netherlands Meteorological Institute, PO Box 201, NL-3730 AE De Bilt, Netherlands.
- V. Fioletov, C. A. McLinden, and C. E. Sioris, Environment Canada, 4905 Dufferin St., Toronto, ON M3H 5T4, Canada. (chris.mclinden@ec.gc.ca)
- N. Krotkov and K. Yang, Laboratory for Atmospheric Chemistry and Dynamics, NASA Goddard Space Flight Center, Code 613.3, Greenbelt, MD 20771, USA.